China Ocean Eng., Vol. 28, No. 5, pp. 599 – 616

DOI 10.1007/s13344-014-0048-x, ISSN 0890-5487

Multi-Fault Diagnosis for Autonomous Underwater Vehicle Based on Fuzzy Weighted Support Vector Domain Description*

ZHANG Ming-jun (张铭钧), WU Juan (吴　娟) and CHU Zhen-zhong (褚振忠)[1]

College of Mechanical and Electrical Engineering, Harbin Engineering University, Harbin 150001, China

(Received 17 December 2012; received revised form 14 October 2013; accepted 20 December 2013)

ABSTRACT

This paper addresses the multi-fault diagnosis problem of thrusters and sensors for autonomous underwater vehicles (AUVs). Traditional support vector domain description (SVDD) has low classification accuracy in the process of AUV multi-fault pattern classification because of the effect of sample sparse density and the uneven distribution of samples, and so on. Thus, a fuzzy weighted support vector domain description (FWSVDD) method based on positive and negative class samples is proposed. In this method, the negative class sample is introduced during classifier training, and the local density and the class weight are introduced for each sample. To improve the multi-fault pattern classifier training speed and fault diagnosis accuracy of FWSVDD, a multi-fault mode classification method based on a hierarchical strategy is proposed. This method adds fault contain detection surface for each thruster and sensor to isolate fault components during fault diagnosis. By considering the problem of pattern classification for a fuzzy sample, which may be located in the overlapping area of hyper-spheres or may not belong to any hyper-sphere in the process of multi-fault classification based on FWSVDD, a relative distance judgment method is given. The effectiveness of the proposed multi-fault diagnosis approach is demonstrated through water tank experiments with an experimental AUV prototype.

Key words: *underwater vehicle*; *support vector domain description*; *multi-fault diagnosis*; *fault classification*

1. Introduction

AUV works in complex marine environments and completes scheduled tasks independently using artificial intelligence, automatic control, pattern recognition, information fusion, system integration, and other technology (Xu and Xiao, 2007). Given the complexity of the marine environment and the high autonomy of AUV, the occurrence of a fault in the AUV will cause significant losses (Xu and Su, 2008). Fault diagnosis technology provides a new method to improve the reliability of AUV systems (Antonelli *et al*., 2004). Scholars have raised numerous methods to address the single fault diagnosis problem of AUV systems and achieved good results in practical application (Zhu *et al*., 2009). However, the rapid development of computers, sensors, and underwater communication technology has made AUV systems more complicated, resulting in the frequent simultaneous occurrence of multiple faults within the system (Li *et al.*, 2005; Hamilton *et al*., 2007). With the unscented Kalman filter to perform the joint estimation of parameters and AUV motion state, a multi-thruster for AUV fault detection was achieved (Lin *et al*., 2011). The multi-sensor fault diagnosis of AUV was achieved

* This project is supported by the National Natural Science Foundation of China (Grant No. 51279040) and the Research Fund for the Doctoral Program of Higher Education of China (Grant No. 20112304110024).

1 Corresponding author. E-mail: chuzhenzhong@hrbeu.edu.cn

by using the node energy difference and feature extraction of wavelet decomposition (Wang *et al*., 2010). However, most of these methods are only suitable for fault diagnosis problems of multi-thruster or multi-sensor and do not consider concurrent problems of thrusters and sensors. When multiple faults simultaneously occur in an AUV system, different fault causes and symptoms result in varying collection or influence domains, making the multi-fault diagnosis of AUV a complex problem. Therefore, a diagnosis study for the concurrent multi-fault of thrusters and sensors in an AUV system and the distinction of thruster and sensor faults are of great significance in improving AUV system security.

In the study of nonlinear system multi-fault diagnosis, commonly used methods include neural networks (Talebi *et al*., 2009), principal component analysis (PCA) (Du and Jin, 2007), support vector machine (SVM) (Gao *et al*., 2007), and other methods. Compared with other nonlinear systems, an AUV system usually has more normal samples and less fault samples. Moreover, fault samples are difficult to be obtained, thus making it difficult for a neural network to obtain a decision-making function with good generalization capability from the limited fault samples (Hu and Wang, 2001). PCA requires that the data samples are mutually independent and follow the Gauss distribution (Li and Xiao, 2011). However, the data samples in an AUV system typically exhibit another type of distribution and have a nonlinear structure. With consideration of the advantages of SVM, such as the capability to solve non-linear problems and small-sized samples (Cheng and Shih, 2007; Peng and Xiao, 2009), this method is more suitable for AUV system multi-fault diagnosis than the neural network and PCA.

Based on SVM, the support vector domain description (SVDD) method was presented (Tax and Duin, 1999). The basic idea of SVDD is to establish the minimum hyper-sphere interface in the kernel feature space and to certain the most number of target samples in the hyper-sphere, while ejecting non-target samples from the hyper-sphere (Khediri *et al*., 2012; Zhang *et al*., 2007; Zhang *et al*., 2009; Zhou *et al*., 2012). However, a study of the multi-fault mode classifier based on the SVDD method reveals the following limitations of this method in the modeling process: (a) the traditional SVDD method treats each sample equally without considering the density of the target data. However, in practice, the importance of each sample is related to the density of the region where the sample is situated; (b) the traditional SVDD method does not consider the uneven sizes of different-fault-mode samples. However, when the sample sizes are not balanced, and the SVDD classification error is undesirably biased toward the class with fewer samples; and (c) the traditional SVDD method does not train non-target class samples together, and the non-target samples will affect the formation of the smallest bounding ball during training. These limitations cause the traditional SVDD method to have low classification accuracy in the process of AUV multi-fault mode classification. According to the sample distribution, Lin and Wang (2002) introduced fuzzy knowledge into the SVDD method and used different penalty coefficients for different samples, such that different samples had different contributions to the objective function. According to the authors' knowledge, only limited open references on the uneven samples size problem and non-target sample learning problem are available.

A multi-fault diagnosis study based on SVM or SVDD needs to establish a multi-mode classifier. The existing multi-mode classifier can be divided into two kinds: direct classifier and indirect classifier. Weston and Watkins (1998) used *k*-SVM to establish a multi-mode classifier directly,

obtaining all classified hyper-planes in one optimization. However, this approach needs to deal with all the learning samples simultaneously and has low learning efficiency. Thus the indirect multi-mode classifier is more commonly used for mode classification. The indirect multi-mode classifier first transforms a multi-classification problem into a series of two-class problems, each of which is then solved (Zhang *et al*., 2009). The typical strategies include the one-to-one strategy (Hsu and Lin, 2002), one-to-many strategy (Han *et al*., 2011), and hierarchical strategy (Schmenker, 2000). For the same N-gram classification problem, the one-to-one strategy needs to establish $N\times(N-1)$ classifiers (Wei *et al*., 2004), whereas one-to-many strategy needs to establish N classifiers (Liu *et al*., 2006). By contrast, the hierarchical strategy, only needs to build $(N-1)$ classifiers at most (Schmenker, 2000). According to the number of classifiers used by different strategies, the hierarchical strategy requires fewer classifiers and has a faster learning and testing speed compared with one-to-one and one-to-many strategies. However, the hierarchical strategy has an accumulative error problem, that is, when misclassification occurs on one layer, the decision-making of the lower layer will be affected. Therefore, the strategy requires that the classifiers near the bottom have higher accuracy.

The SVDD method uses the kernel function to project the original problem into an unknown high-dimensional space, which will cause a lack of association among the feature spaces of each hyper-sphere. Thus, in the process of multi-fault mode classification, sample points may be located in the overlapping area of hyper-spheres or may not belong to any hyper-sphere. The unknown fault mode for these sample points cannot be directly determined based on the distances obtained by different hyper-sphere classification boundaries. The study of the class ownership judgment of fuzzy sample points can improve the accuracy of a fault diagnosis system.

In this paper, the FWSVDD method based on positive and negative class samples is proposed for the establishment of an AUV multi-fault mode classifier. Unlike the traditional SVDD method, the proposed method introduces negative class samples (not target samples) during the classifier training to enable the SVDD problem to be distinguished between the positive and negative class samples. The proposed method introduces a local density and class weight for each sample, increases the importance of the data on the high-density distribution region, and makes the classification boundary more compact. A multi-fault mode classification method based on the hierarchical strategy is proposed. This method adds the fault contain detection surface (FCDS) for each thruster and sensor to isolate the fault components during fault diagnosis. Fault mode classification is then performed for the components. For the sample points outside the FCDS, the inclusion degree threshold method is proposed for the class ownership judgment to improve classification accuracy. For the class ownership problem of fuzzy sample points, a relative distance judgment method is given. Finally, water tank experimental verification is conducted using an experimental AUV prototype.

This paper is organized as follows: Section 2 introduces the fuzzy weighted support vector domain description method. Section 3 presents the AUV multi-fault classification method based on hierarchical strategy classification. Section 4 discusses the class ownership judgement method of fuzzy sample points. Section 5 verifies feasibility and effectiveness of the proposed approach through experiments. Finally, a brief conclusion is drawn in Section 6.

2. FWSVDD Method

2.1 FWSVDD Classifier

To describe the local density of the data sample distribution, we introduce local density ρ_i ($0\leq\rho_i\leq1$) for each data sample x_i based on the clustering method (Cristianini and Shawe-Taylor, 2004). A larger ρ_i denotes that the data sample is more important and thus accounts for larger weight in the process of building the classifier. In this work, ρ_i is equivalent to the fuzzy factor, the selection method of which will be given in Section 2.2. By introducing ρ_i, the traditional SVDD can be extended to the fuzzy SVDD.

In the process of classification modeling, we introduce a local density for each data sample and give data set $X=\{(x_1, \rho_1), \ldots, (x_M, \rho_M)\}$ with a local density coefficient given that the local density of similar samples differs from that of non-similar samples. In this paper, the nonlinear mapping theory (Cristianini and Shawe-Taylor, 2004) is taken as a reference to define a fuzzy nonlinear mapping Φ: $(X, \rho)\rightarrow F$, namely, $(X, \rho)\rightarrow\Phi(X, \rho)=\rho\Phi(X)$. This fuzzy nonlinear mapping enables the adjustment of the weight of the sample data in the nonlinear mapping to obtain the data set $\{\rho_1\Phi(x_1), \rho_2\Phi(x_2), \ldots, \rho_M\Phi(x_M)\}$ corresponding to $\{(x_1, \rho_1), (x_2, \rho_2), \ldots, (x_M, \rho_M)\}$ in the high-dimensional space. The inner product operation in the high-dimensional space can be written as:

$$\Phi(x_{\bar{i}}, \rho_{\bar{i}})\Phi(x_{\bar{j}}, \rho_{\bar{j}}) = \rho_{\bar{i}}\Phi(x_{\bar{i}})\rho_{\bar{j}}\Phi(x_{\bar{j}}) = \rho_{\bar{i}}\rho_{\bar{j}}\Phi(x_{\bar{i}})\Phi(x_{\bar{j}}), \quad \bar{i}, \bar{j} = 1, 2, \ldots, M. \tag{1}$$

In the process of AUV multi-fault classification based on SVDD, positive samples (target samples) $X_{\text{target}}=\{(x_i, \rho_i), i=1, 2, \ldots, n\}$ and negative samples (non-target samples) $X_{\text{outlier}}=\{(x_j, \rho_j), j=1, 2, \ldots, m\}$ are selected for simultaneous classifier training to improve the anti-noise-interference capability of the classification boundary. n denotes the number of positive samples, whereas m stands for the number of negative samples. As the positive and negative samples have different numbers, a class weight value s is added for each class sample to obtain the FWSVDD based on the positive and negative samples. The class weight s will be given in Section 2.2.

Given that the non-target samples are increased and the local density is introduced to each sample, the optimization problem to be solved can be expressed as:

$$\begin{aligned} &\min_{R,a,\varepsilon_i}(R^2 + C_1\sum_{i=1}^{n}s_i\varepsilon_i + C_2\sum_{j=1}^{m}s_j\varepsilon_j);\\ &\text{s.t.} \quad \begin{cases} \left\|\Phi(x_i, \rho_i) - a\right\|^2 \leq R^2 + \varepsilon_i \quad , \quad \varepsilon_i \geq 0, \ i = 1, 2, \ldots, n \\ \left\|\Phi(x_j, \rho_j) - a\right\|^2 \geq R^2 - \varepsilon_j \quad , \quad \varepsilon_j \geq 0, \ j = 1, 2, \ldots, m \end{cases} \end{aligned} \tag{2}$$

where, R is the hyper-sphere radius. $C_1>0$ and $C_2>0$ are the penalty coefficients for balancing the size of the smallest bounding hyper-sphere and the number of negative (or positive) samples inside (outside) the hyper-sphere; $\varepsilon>0$ is the slack variable; s_i and s_j are the class weight values of samples; ρ_i and ρ_j are the local density of the samples; a is the center of the hyper-sphere.

Eq. (2) is transformed into a Lagrange extreme problem as follows:

$$L(R,a,\alpha_i,\gamma_i,\varepsilon_i,\alpha_j,\gamma_j,\varepsilon_j)=R^2+C_1\sum_{i=1}^{n}s_i\varepsilon_i+C_2\sum_{j=1}^{m}s_j\varepsilon_j-\sum_{i=1}^{n}\gamma_i\varepsilon_i-\sum_{j=1}^{m}\gamma_j\varepsilon_j$$
$$-\sum_{i=1}^{n}\alpha_i\left(R^2+\varepsilon_i-\left\|\Phi(x_i,\rho_i)-a\right\|^2\right)-\sum_{j=1}^{m}\alpha_j\left(\left\|\Phi(x_j,\rho_j)-a\right\|^2-R^2+\varepsilon_j\right), \tag{3}$$

where, $\alpha_i\geq 0$, $\gamma_i\geq 0$, $\alpha_j\geq 0$, and $\gamma_j\geq 0$ are the Lagrange multipliers.

Let the partial derivative of R, a, ε_i, and ε_j in Eq. (3) be equal to zero to derive the dual problem:

$$L(R,a,\alpha_i,\gamma_i,\varepsilon_i,\alpha_j,\gamma_j,\varepsilon_j)=\sum_{i\in P}\alpha_i\rho_i^2K(x_i,x_i)-\sum_{j\in N}\alpha_j\rho_j^2K(x_j,x_j)$$
$$-\sum_{i\in P}\sum_{l\in P}\alpha_i\alpha_l\rho_i\rho_lK(x_i,x_l)-\sum_{j\in N}\sum_{k\in N}\alpha_j\alpha_k\rho_j\rho_kK(x_j,x_k)+2\sum_{i\in P}\sum_{j\in N}\alpha_i\alpha_j\rho_i\rho_jK(x_i,x_j), \tag{4}$$

where, P indicates that x belongs to positive class samples, N indicates that x belongs to negative class samples, $K(x_i, x_j)=\exp[-\|x_i-x_j\|^2/(2\sigma^2)]$ is the kernel function, and σ is the kernel parameter.

The label of positive class samples is +1, and the label of negative class samples is −1, such that

$$y_i=\begin{cases}+1 & x_i\in P\\ -1 & x_i\in N\end{cases} \tag{5}$$

$$\alpha_i'=y_i\alpha_i;$$

$$\min\sum_{i\in P,N}\alpha_i'\rho_i^2K(x_i,x_i)-\sum_{i\in P,N}\sum_{j\in P,N}\alpha_i'\alpha_j'\rho_i\rho_jK(x_i,x_j); \tag{6}$$

$$\text{s.t.}\quad\begin{cases}0\leq\alpha_i\leq C_1s_i & i\in P\\ 0\leq\alpha_j\leq C_2s_j & j\in N\end{cases} \tag{7}$$

The dual problem obtained from using the Lagrange multiplier to transform the FWSVDD method proposed in this paper, which is based on positive and negative class samples, is similar to the traditional SVDD method in terms of the formula. However, these formulas have essential differences between them. Given that the local density and class weight are introduced for the positive and negative samples in FWSVDD method, the importance of the high-density region sample is increased and the imbalance of the number of differently classed samples is reduced.

When a new sample point x_{test} should be identified, the distance between the new sample point and the center of the hyper-sphere is calculated as:

$$f^2=\left\|\Phi(x_{\text{test}},\rho_{\text{test}})-a\right\|^2$$
$$=K(x_{\text{test}},x_{\text{test}})-2\sum_{i\in P,N}\alpha_i'\rho_{\text{test}}\rho_iK(x_{\text{test}},x_i)+\sum_{i\in P,N}\sum_{j\in P,N}\alpha_i'\alpha_j'\rho_i\rho_jK(x_i,x_j), \tag{8}$$

where, ρ_{test} is the local density of the sample points to be identified.

If $f^2<R^2$, then the new sample points to be identified belong to the hyper-sphere; otherwise, they do not belong to the hyper-sphere.

2.2 Determination of Local Density and Class Weight Value

The density of the region of each sample point differs in terms of the multi-fault mode classification process. Given the different local densities of sample points between different regions, the importance of each sample point for different faults varies. The target data in high-density region are more important than the data in the low-density region and should thus be included within the hyper-sphere. To describe

the importance degree of the data sample, we introduce local density ρ_i for data sample x_i.

To determine the local density ρ_i of the i-th sample point x_i, the nearest neighbor method is adopted (Hao and Jiang, 2007). In the solving process, the distance $d(x_i, x_i^l)$ between each sample point x_i and sample x_i^l nearest to x_i is calculated, and then the average distance ζ of all sample points from their respective nearest sample points is calculated. The local density ρ_i of sample point x_i is given by

$$\rho_i = \exp\left[\zeta \Big/ d\left(x_i, x_i^l\right)\right], \quad i = 1,\ 2,\ ...,\ n^k; \tag{9}$$

$$\zeta = \sum_{i=1}^{n^k} d\left(x_i, x_i^l\right) \Big/ n^k, \tag{10}$$

where n^k is the number of the samples that belong to class k.

In the modeling of the fault mode classifier, when the positive and negative class samples are trained simultaneously and if the numbers of positive and negative class samples are unbalanced, the classification errors tend toward those of the small-sized sample. In order to reduce this effect, we introduce different weights for each class sample according to the number of the samples in the paper, which can reflect the importance of different types of samples in the classifier learning. Suppose that the total number of the training samples is T and the sample number belonging to Class k is n^k, and then the weight value of class k is

$$s^k = 1 - n^k / T. \tag{11}$$

The analysis of Eq. (11) reveals that when the sample number of class k_1 is smaller than that of class k_2, then $s_{k_1} > s_{k_2}$. By adjusting the class weights, the effect of the class with small-sized samples on the classifier can be increased, thereby reducing the misclassification problem caused by the unbalanced sample numbers.

3. AUV Multi-Fault Classification Based on the Hierarchical Strategy

In the AUV fault modeling process, under the conditions of the same kernel parameters and penalty coefficient, the model is established based on the FWSVDD method for the sample data of a thruster or sensor of the AUV in a single fault mode to obtain L hyper-spheres that represent different fault modes. Based on the overall sample data of the training samples of L hyper-spheres, a larger hyper-sphere containing L fault modes is trained to build L+1 hyper-spheres (S_1, …, S_l, …, S_L, S_{L+1}). (S_1, …, S_l, …, S_L) represent L fault modes F_1, …, F_l, …, F_L, respectively, which is called the multiclass interface of the multi-fault mode. The hyper-sphere S_{L+1} contains all fault mode samples {F_1, …, F_l, …, F_L}, which comprise the FCDS. The distance from x to the S_{L+1} center is calculated upon the arrival of the new sample point x.

$$\begin{aligned} f_{x(L+1)}{}^2 &= \left\| \Phi\left(x, \rho\right) - a_{(L+1)} \right\|^2 \\ &= \rho^2 K\left(x, x\right) - 2\sum_i \alpha_i^{(L+1)\prime} \rho_i^{(L+1)} \rho^{(L+1)} K\left(x, x_i^{(L+1)}\right) \\ &+ \sum_i \sum_j \alpha_i^{(L+1)\prime} \alpha_j^{(L+1)\prime} \rho_i^{(L+1)} \rho_j^{(L+1)} K\left(x_i^{(L+1)}, x_j^{(L+1)}\right). \end{aligned} \tag{12}$$

If $f_{x(L+1)}{}^2 \le r_{(L+1)}{}^2$, x belongs to FCDS which is represented by S_{L+1}. We then calculate the distance

from x to the l-th hyper-sphere center, which is in the FCDS S_{L+1}, l=1, …, L. If f_{xl}^2 is smaller than the radius of the l-th hyper-sphere, x belongs to the l-th type fault mode represented by S_l; otherwise, x belongs to the other fault type.

In practice, AUV is disturbed by ocean currents and other external disturbances. Thus, the existing noise in the sensor data may cause some fault sample points to locate beyond the FCDS S_{L+1}, resulting in a fault leakage diagnosis. Thus, the appropriate mode classification cannot be performed for the fault. To this end, the inclusion degree threshold is proposed for the class ownership judgment problems of the new sample points. When the new sample point needs to be determined to which class it belongs, we first determine whether the sample point is located within the fault FCDS or not. If the sample point is outside the FCDS, the inclusion degree R_{reject}^{L+1} is calculated based on the new sample point to the FCDS S_{L+1} according to Eq. (13), and the inclusion degree is then compared with the pre-set threshold η. If the inclusion degree $R_{\text{reject}}^{L+1} > \eta$, the new sample point belongs to the fault type represented by the FCDS of the thruster or the sensor; otherwise, it belongs to other fault types. In order to balance the proportion of samples that do and do not belong, we generally set the threshold $\eta \in [0.9, 1]$.

$$R_{\text{reject}}^{L+1} = \begin{cases} 1 & R_{L+1} \geq f \\ R_{L+1}/f & R_{L+1} < f \end{cases} \tag{13}$$

where f is the distance from the new sample point to S_{L+1} center, which can be calculated by Eq. (12). R_{L+1} is the S_{L+1} radius.

4. Class Ownership Judgment of Fuzzy Sample Points

For the SVDD model, we give sample point x and calculate the distance f_{xl}^2 from point x to hyper-sphere center according to Eq. (8). Compared with the corresponding R_l^2, the number b of hyper-spheres containing sample points x can be determined. According to different values of b, we analyze the following cases.

4.1 Case for b=1

In this case, point x is only located within a classification hyper-sphere and point x belonging to this fault mode is represented by the hyper-sphere. Thus, we can directly determine the class ownership.

4.2 Case for b=0

This case shows that the sample point x is located outside the feature space formed by all hyper-spheres that have a defined fault classification and do not belong to any fault category, as shown in Fig. 1.

When the sample point is located between two hyper-spheres, the best classification surface established by the traditional method is the center position P between the two spherical surfaces, as shown in Fig. 1a. When the sample points are located on both sides of P, they belong to S_1 and S_2. When sample points are located within P, the probability that these sample points belong to the fault modes represented by S_1 and S_2 is 0.5. However, when the two hyper-sphere radii are not the same, the

sparsity of sample distribution represented also differs. If the best classification surface P is set in the middle of the two hyper-spheres according to the traditional method, sparse sample distribution S_1 is unreasonable. Therefore, we propose an improved strategy based on the relative distance, as shown in Fig. 1b. First, a line is drawn over the two hyper-sphere centers, and the line segment between the two intersections of the line and the two hyper-spheres is divided by R_1/R_2. Thus, we obtain the best classification surface P'.

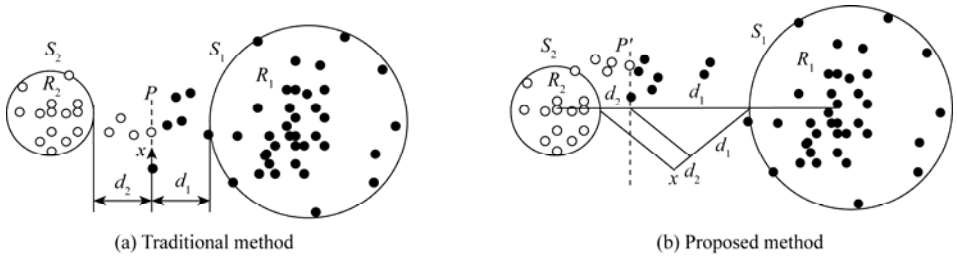

Fig. 1. Sample point ownership judgment when b=0.

In order to verify the effectiveness of the improved strategy, we select 100 sample points in the classification surface P and P' for classification experiments. We set the two hyper-sphere centers as R_1 and R_2 and $R_1 \neq R_2$, $R_1 \geq R_2$. We gradually increase the hyper-sphere radius ratio R_1/R_2 in the experiment. The average probabilities that the sample point belongs to the fault mode represented by S_1 based on the two methods are shown in Table 1. The probability that sample point x belongs to S_1 increases with the increasing R_1/R_2 before the method is improved. However, in the improved method, the average probabilities are all approximately 0.5. The experimental results show that the improved classification surface P' reflects uneven distribution problems of the sample between the two categories and is reasonably removed from the larger hyper-sphere, where the samples distribute loosely.

Table 1 Probability of x belonging to the larger hyper-sphere R_1 when b=0

R_1/R_2	1	2	4	8	10	15	20
Traditional strategy	0.502	0.520	0.594	0.673	0.720	0.791	0.852
Improved strategy	0.500	0.502	0.502	0.503	0.500	0.510	0.518

4.3 Case for b>1

This case shows that the sample point x is in the overlap area of the multiple classification hyper-spheres, as shown in Fig. 2.

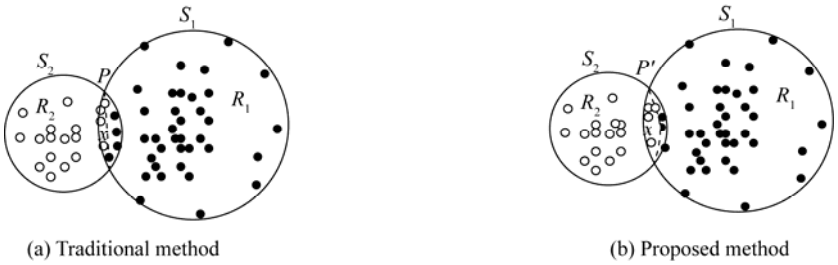

Fig. 2. Sample point ownership judgment when b>1.

For this case, the traditional judgment method uses the plane constructed by the intersecting lines

of two hyper-spheres as the best classification surface P as shown in Fig. 2a. When the sample points are located on both sides of P, they belong to S_1 and S_2. When sample points are located within P, the probabilities that the sample points belong to the fault modes represented by S_1 and S_2 are 0.5. However, this classification method is unreasonable for a small ball, where the samples are distributed more densely. Therefore, the improved strategy based on the relative distance is proposed in this paper, as shown in Fig. 2b. The plane $(R_1-d_1)/R_1=(R_2-d_2)/R_2$ is constructed over the intersection point of the two hyper-spheres to derive the best classification surface P' where, d_1 and d_2 are the distances from the sample point to the hyper-sphere center.

In order to prove the effectiveness of the proposed method, 100 sample points in the classification surface P and P' are selected for classification experiments. With the increase of the two hyper-sphere radius ratio R_1/R_2, the average probabilities that a sample point belongs to the fault mode represented by S_1 from the two methods are shown in Table 2. The probabilities that a sample point in the classification surface P belongs to the fault mode represented by S_1 decrease with the increasing of R_1/R_2 before the method is improved. However, when the classification surface P' is used for classification, the probabilities are approximately 0.5 with the increasing R_1/R_2. The experimental results show that the improved classification surface P' reflects the uneven distribution problems of the sample between the two categories and is reasonably removed near the larger hyper-sphere in which samples distribute loosely.

Table 2 Probabilities of x belonging to the larger hyper-sphere R_1 when $b>1$

R_1/R_2	1	2	4	8	10	15	20
Traditional strategy	0.500	0.499	0.467	0.446	0.303	0.222	0.148
Improved strategy	0.500	0.501	0.500	0.500	0.500	0.510	0.512

In summary, the proposed fuzzy sample point class ownership judgment method based on the relative distance is expressed as:

$$\theta=\begin{cases} f_{xl}^{\ 2}/R_l^2 & b=1 \\ \min\left[\left(f_{xl}^{\ 2}-R_l^2\right)/R_l^2\right] & b=0 \\ \min\left[\left(R_l^2-f_{xl}^{\ 2}\right)/R_l^2\right] & b>1 \end{cases} \qquad l=1,\ 2,\ \ldots,\ L\,. \tag{14}$$

In the process of the judgment, the distances d_l from the sample point x to the center of each hyper-sphere are calculated. According to different values b of the hyper-sphere containing sample point x, Eq. (14) is used to calculate the relative distance θ from the sample point to the corresponding fault mode hyper-sphere center. The hyper-sphere to which θ is the smallest is taken as the fault mode for the sample point. If the sample point is located in the classification surface of two hyper-spheres P', then the sample point belongs to the two fault modes.

5. Experiments

5.1 Experimental Conditions

In order to validate the effectiveness of the proposed FWSVDD in the pattern classification and

AUV multi-fault diagnosis, the "Beaver" AUV test prototype shown in Fig. 3 is used for the fault simulation experiments in a pool environment. Fig. 4a illustrates the hardware control architecture for "Beaver" AUV, and Fig. 4b illustrates the software control architecture for "Beaver" AUV.

Fig. 3. "Beaver" AUV test prototype.

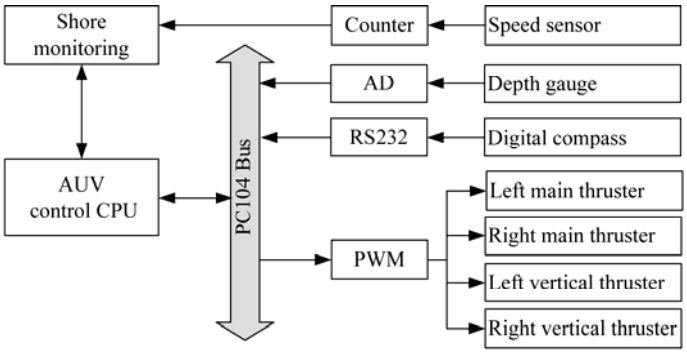

(a) Hardware control architecture of the "Beaver" AUV

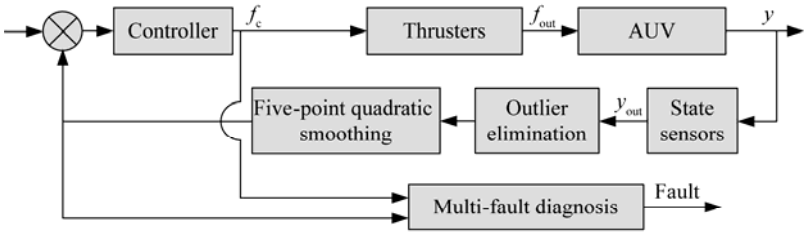

(b) Software control architecture of the "Beaver" AUV

Fig. 4. Control architecture of the "Beaver" AUV.

The actual faults are difficult to mimic under the pool condition. Thus, the soft simulation method is adopted to mimic the faults by analyzing the fault types of sensors and thrusters such that the data can be used to demonstrate the efficiency of the proposed fault diagnosis algorithm.

Different fault types occur on AUV sensors: no output, drift output, and unpermitted deviation (Zhu *et al*., 2009). The following fault model can be used to describe different fault types (Qi and Han,

2009):

(1) Stuck fault model: $y_{out}=\alpha$, where α is constant, and y_{out} is the state measured by sensor;

(2) Constant gain fault model: $y_{out}=\beta y$, where β is the constant gain coefficient, and y is the real AUV state;

(3) Constant bias fault model: $y_{out}=y+\Delta$, where Δ is constant; and

(4) Drift fault model: $y_{out}=y+\Lambda$, where the value of Λ changes over time.

Based on the above fault models, this paper sets different values of α, β, Δ, and Λ and then substitute y with y_{out} in AUV controller design. Thus, sensor fault is realized via soft simulation.

Different fault types occur on AUV thrusters: stuck, blade drop, and blade fracture. Thruster faults can also be described using models similar to those of sensor faults. However, the thruster faults differ from the sensor faults, which cannot be compensated autonomously, because the controller can ensure the AUV real-time track target value during AUV operation. An AUV can also track the target value even under a thruster fault condition via the close-loop control when the thruster fault is small. However, an AUV cannot track the target value in the presence of thruster saturation if the thruster fault is large. Thus, this paper classifies thruster faults as compensable and uncompensated faults depending on whether an AUV can track the target value when thruster fault occurs. When thruster fault occurs, the actual thruster f_{out} would be smaller than theoretical thruster f_c, such that the fault model can be described as $f_{out}=f_c-\Delta$, where Δ is the thruster fault, and $\Delta \cdot f_{out}>0$. Owing to the existence of saturated thruster f_0, the magnitude of Δ determines the type of thruster fault, i.e., when $f_c=f_{out}+\Delta>f_0$, the fault would be an uncompensated fault, and vice versa. During experiments, the value of Δ can be set beforehand, and the output of controller f_c can be substituted with $f_{out}=f_c-\Delta$, such that thruster fault can be realized via soft simulation.

5.2 Performance Verification for Fuzzy Weighted SVDD Method

In order to validate the effectiveness in building classifier model and the accuracy in pattern classification of FWSVDD method based on positive and negative class samples, the constant gain fault $u=0.8u_r$ is simulated in the surge speed sensor of "BEAVER" test prototype. The fault time lasts from Beat 150 to Beat 250. Where, u_r is the actual surge speed and u is the surge speed used in controller. The time of the control beat is 0.2 s. Based on the AUV control variable and state variable data from the experiments, the original characteristic indexes that include the detailed and observed residual signals are processed using the wavelet coefficient fusion method and neural network observer in Zhang *et al*. (2010), as shown in Fig. 5. The detailed residual contains the details of the original signal lost during wavelet coefficient reconstruction, whereas the observed residual is the deviation between the measured values of sensors and the output values of the observer.

The original characteristic indexes from Beat 201 to Beat 400 are selected as learning samples. Fifty groups of fault samples from Beat 201 to Beat 250 are negative class samples with a label of −1. One-hundred fifty groups of normal samples from Beat 251 to Beat 400 are positive class samples with a label of 1. Selecting the same kernel parameter $\sigma=0.5$ and the same penalty coefficients $C_1=C_2=2.0$, optimized solving is performed based on the FWSVDD and traditional SVDD methods to obtain the classifier model shown in Fig. 6. The thick solid line in Fig. 6 denotes the model boundary obtained by

the traditional SVDD method, whereas the thin dotted line is the model boundary obtained by the FWSVDD method.

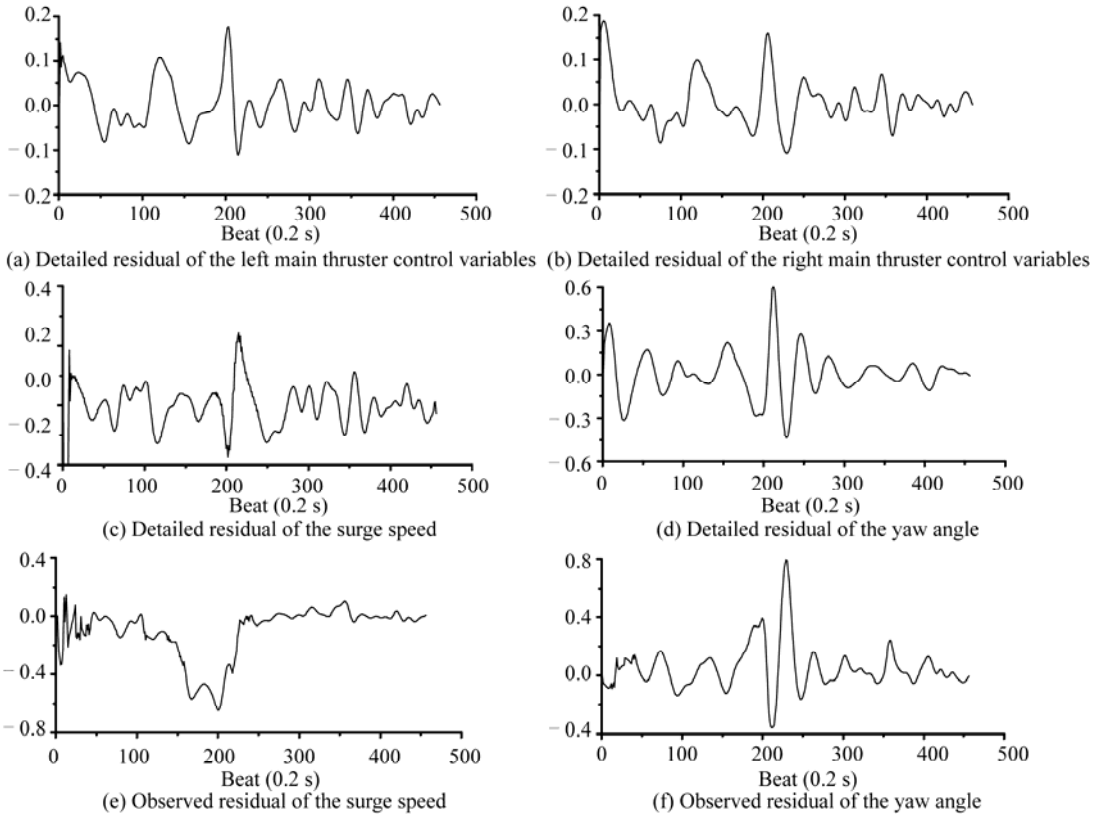

Fig. 5. Original characteristic indexes.

In Fig. 6, the hyper-sphere radius obtained from the SVDD method is 0.915, whereas the radius obtained from the FWSVDD method is 0.887. The results show that the classifier model boundary established by the FWSVDD method is more compact and surrounds the target sample better than that established by the SVDD method.

In order to validate the accuracy of the established classifier model in terms of the pattern classification, the data between Beat 151 and Beat 200 are selected for validation, as shown in Fig. 5. The distances from the sample point to the two feature sphere centers are calculated according to Eq. (8), as shown in Fig. 7. Where, '+' is obtained by the FWSVDD classifier model, whereas '*' is obtained by the SVDD classifier model. The thick solid line denotes the hyper-sphere radius from the traditional method, whereas the thin dashed line denotes the hyper-sphere radius from the proposed method.

For the selected 50 groups of testing samples in Fig. 7, the SVDD method misjudges four sample points, and the classification accuracy is 92%. The proposed method misjudges two sample points, and the classification accuracy is 96%. By comparing the experimental results, the FWSVDD method classifier model can obtain more compact classifier hyper-sphere boundary surface after adding the

non-target samples and introducing the local density and category weights of samples, improving the classification accuracy by 4%. The experimental results show that the proposed FWSVDD method based on positive and negative class samples can effectively build the classifier model and has higher accuracy in pattern classification.

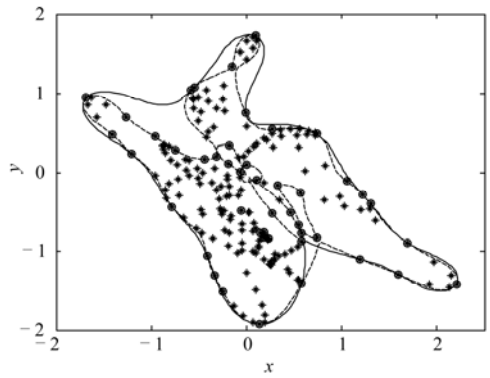

Fig. 6. Modeling comparison of the proposed method with the traditional method.

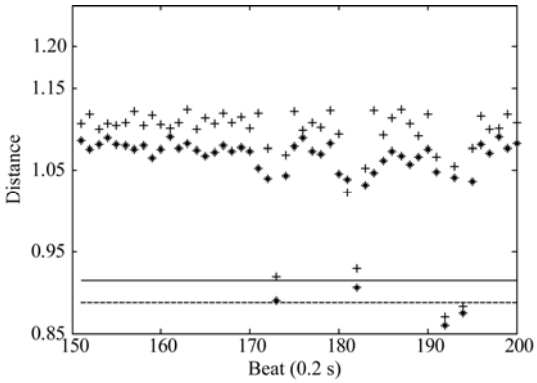

Fig. 7. Distance from the test sample point to the feature sphere center.

5.3 AUV Multi-Fault Diagnosis Experiments

In order to validate the effectiveness of AUV multi-fault classification method based on the FWSVDD method, the compensable concurrent fault of the right main thruster and the constant deviation fault of the angle sensor are simulated by "BEAVER". The fault of the right main thruster is $f_{out}=0.9f_c$ and the fault of angle sensor is $\varphi=\varphi_r-15^o$. The fault has lasted from 48 s to the end of the experiment. φ_r is the actual yaw angle, and φ is the yaw angle used in controller. For the compensable fault $f_{out}=0.9f_c$, the fault leakage diagnosis is generated easily by external interference because the fault is small. For the constant deviation fault of the angle sensor, the yaw angle mutates only at 48 s, and the motion controller then controls the AUV yaw angle sensor output value to follow the desired goals, causing the AUV status change attributed to the fault to be similar to the external interference. The results of the thruster control signal and the state variable from the water tank experiments are shown in Fig. 8. The thick solid line in Fig. 8 denotes the control signal of the left main thruster and the thin dashed line is the control signal of the right main thruster. For the above simulated fault, multi-fault diagnosis aims to locate the thruster and sensor with fault, as well as to identify the fault mode.

As the AUV engages in the level motion, the fault diagnosis of the left and right main thrusters, the longitudinal velocity sensor, and the yaw angle sensor is considered, and the adopted contain detection surface includes the normal state contain detection surface as well as the FCDS of the left main thruster, the right main thruster, the yaw angle sensor, and the longitudinal velocity sensor. The class ownership analysis of sample points is performed on the experimental data shown in Fig. 8. The inclusion degree from the sample points to the AUV normal state hyper-sphere and the FCDS of each thruster and sensor is calculated according to Eqs. (12) and (13), as shown in Fig. 9. The inclusion degree threshold in the process of fault diagnosis is set as $\eta=0.95$, which is denoted by dotted lines.

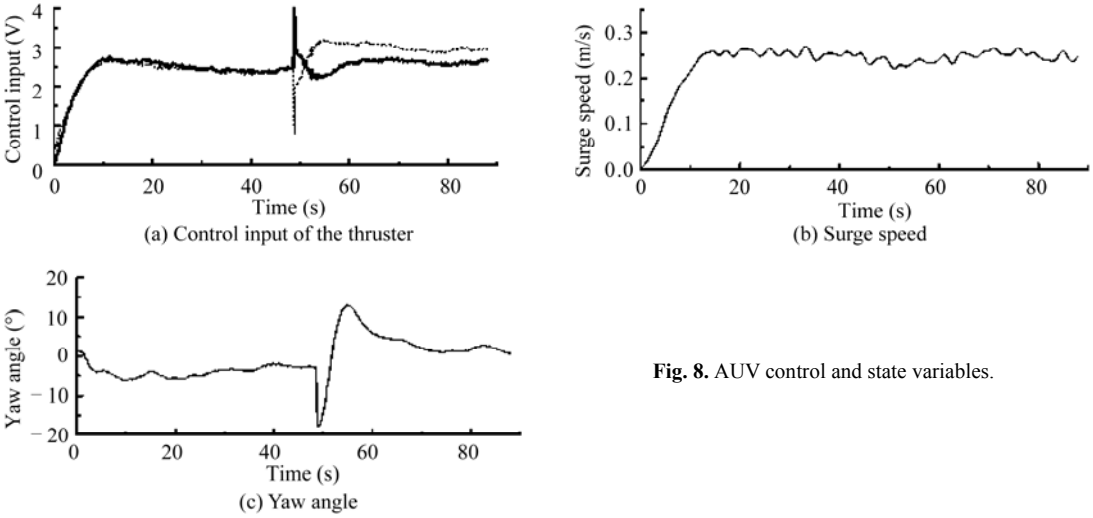

Fig. 8. AUV control and state variables.

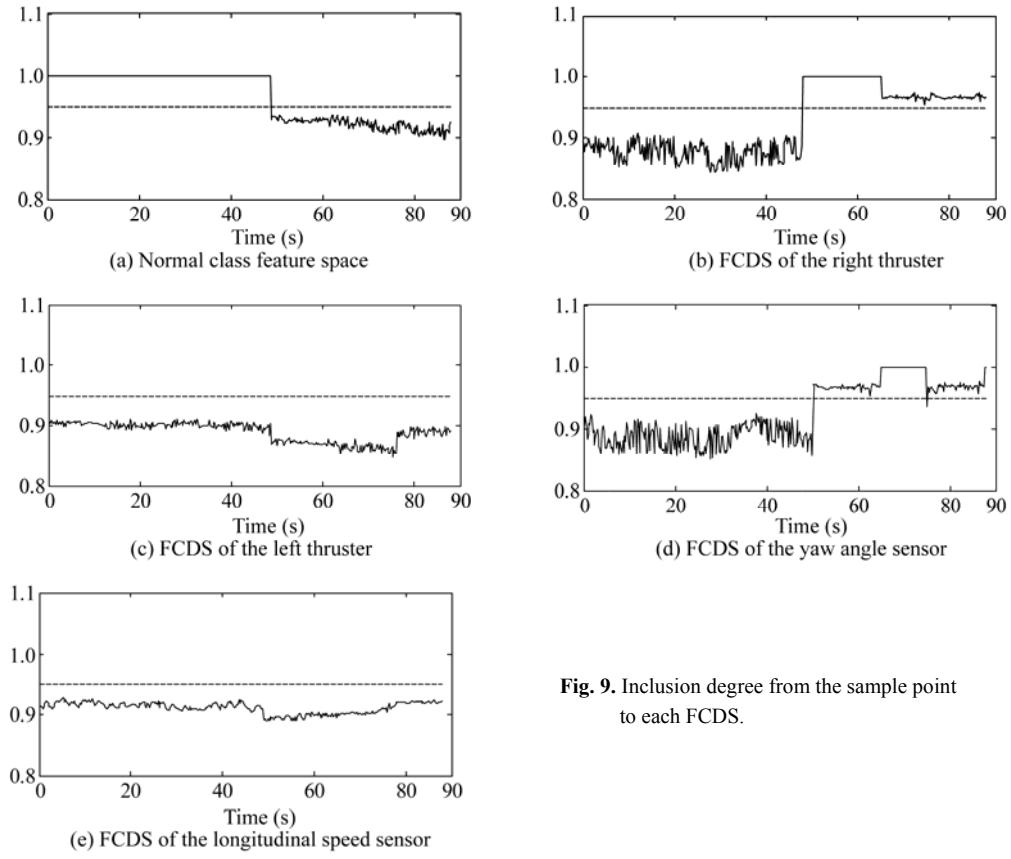

Fig. 9. Inclusion degree from the sample point to each FCDS.

From the inclusion degree of sample points shown in Fig. 9 to the FCDS of each thruster and sensor, we find that the inclusion degree from the sample points to the AUV normal mode is 1, and the inclusion degree to each thruster and sensor is smaller than 0.95 before 48.8 s. The inclusion degree

from 196 sample points to the normal mode is smaller than 0.95 between 48.8 s and 88 s, which shows that the AUV is in normal operation before 48.8 s. The inclusion degree from 83 sample points to the FCDS of the right main thruster is 1 between 48.8 s and 65 s. According to the proposed sample point judgment strategy, these sample points belong to the right main thruster fault. Between 65 s and 75 s, the inclusion degree from 50 sample points to the FCDS of angle sensor is 1. These sample points belong to the angle sensor fault. Between 48.8 s and 88 s, the inclusion degree from all of the sample points to the FCDS of the right main thruster and the angle sensor is larger than 0.95, and the inclusion degree to the FCDS of the left main thruster and the longitudinal speed sensor fault components is smaller than 0.95. According to the proposed sample point judgment strategy, the AUV system has a fault in the right main thruster and the angle sensor.

After the detection of fault location, the fault modes of the right main thruster and the angle sensor are further analyzed. For the thruster fault, fault modes mainly include the compensable and uncompensated fault. For the sensor fault, the fault modes mainly include constant deviation fault, constant gain fault, drift fault, and stuck fault. According to Eq. (14), the distances from sample points to their corresponding fault mode hyper-sphere center are shown in Fig. 10.

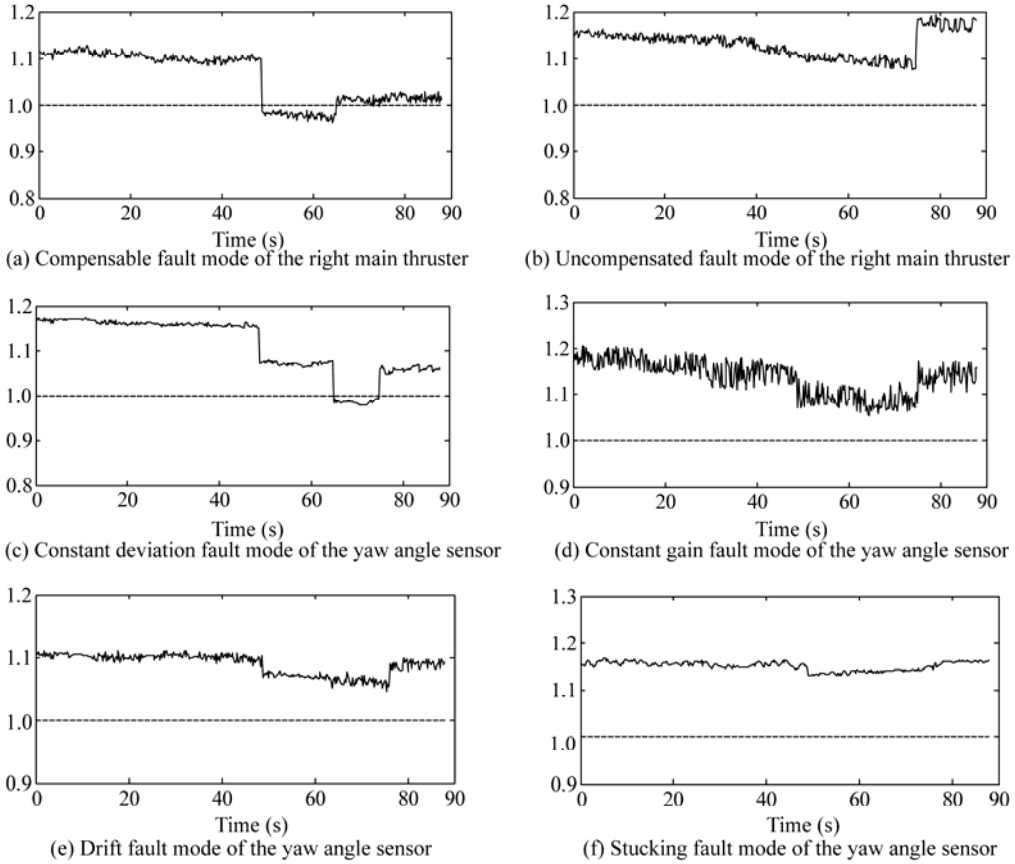

Fig. 10. Fault mode classification results.

Given that the fault of the AUV thruster and sensor is detected from 48.8 s, 196 sample points between 48.8 s and 88 s are selected for analysis in the fault mode classification. From the fault mode classification results in Fig. 10, among the 196 sample points between 48.8 s and 88s, the relative distances from 42.13% of the sample points to the compensable fault mode of the right main thruster are smaller than 1, and the distances from 25.38% of the sample points to the constant deviation fault mode of angle sensor are smaller than 1. Other sample points located between these two fault modes' hyper-spheres are classified as fuzzy sample points. According to the proposed fuzzy sample point judgment strategy used to calculate the class attribution, 10.77% of the sample points belong to the compensable fault mode of the right main thruster, 16.92% of the sample points belong to the constant deviation fault mode of the angle sensor, and 72.31% of the sample points belong to the two fault modes that can determine the kind of fault modes that occur in the AUV. Experimental results show that the AUV multi-fault diagnosis results using the proposed FWSVDD method based on the positive and negative classes are consistent with actual fault conditions. The experimental results verify the effectiveness of the AUV multi-fault mode classification method proposed in this paper.

6. Conclusion

In this paper, we study the AUV multi-fault pattern classification problem based on the FWSVDD method and present the selection method for the local density and the class weight of samples. In the process of the unknown sample point judgment based on the classification model, a hierarchical strategy classification method is proposed. In consideration of the class ownership and judgment problem for fuzzy sample points that are in the overlapping area of hyper-spheres or that do not belong to any hyper-sphere in the process of fault classification, a relative distance judgment method is established. Experimental results obtained from water tank experiments using an AUV test prototype show that the FWSVDD method based on the positive and negative class samples modeling proposed in this paper has higher classification accuracy than traditional SVDD methods do. The proposed method effectively accomplishes the multi-fault mode classification in the case where the compensable fault of the thruster and constant deviation fault of the AUV sensor occurs simultaneously.

References

Antonelli, G., Caccavale, F., Sansone, C. and Villani, L., 2004. Fault diagnosis for AUVs using support vector machines, *Proceedings of the 2004 IEEE International Conference on Robotics & Autonomation*, New Orleans, 4486−4491.

Cheng, S. X. and Shih, F. Y., 2007. An improved incremental training algorithm for support vector machines using active query, *Pattern Recognition*, **40**(3): 964−971.

Cristianini, N. and Shawe-Taylor, J., 2004. *An Introduction to Support Vector Machines and Other Kernel-Based Learning Methods*, Cambridge, Cambridge University Press, 33−40.

Du, Z. M. and Jin, X. Q., 2007. Detection and diagnosis for multiple faults in VAV systems, *Energy and Building*, **39**(8): 923−934.

Gao, G. H., Zhang, Y. Z., Zhu, Y. and Duan, G. H., 2007. Hybrid support vector machines-based multi-fault

classification, *Journal of China University of Mining and Technology*, **17**(2): 246−250.

Hamilton, K., Lane, D. M., Brown, K. E., Evans, J. and Taylor, N. K., 2007. An integrated diagnostic architecture for autonomous underwater vehicles, *Journal of Field Robotics*, **24**(6): 497−526.

Han, H., Gu, B., Hong, Y. C. and Kang, J., 2011. Automated FDD of multiple-simultaneous faults (MSF) and the application to building chillers, *Energy and Buildings*, **43**(9): 2524−2532.

Hao, H. W. and Jiang, R. R., 2007. Training sample selection method for neural networks based on nearest neighbor rule, *Acta Automatica Sinica*, **33**(12): 1247−1251. (in Chinese)

Hsu, C. W. and Lin, C. J., 2002. A comparison of methods for multi-class support vector machines, *IEEE Transactions on Neural Networks*, **13**(2): 415−425.

Hu, S. S. and Wang, Y., 2001. Support vector machine based fault diagnosis for nonlinear dynamics systems, *Control and Decision*, **16**(5): 617−620. (in Chinese)

Khediri, I. B., Weihs, C. and Limam, M., 2012. Kernel k-means clustering based local support vector domain description fault detection of multimodal processes, *Expert Systems with Applications*, **39**(2): 2166−2171.

Li, H. and Xiao. D. Y., 2011. Survey on data driven fault diagnosis methods, *Control and Decision*, **26**(1): 1−10. (in Chinese)

Li, J. H., Jun, B. H., Lee, P. M. and Hong, S. W., 2005. A hierarchical real-time control architecture for a semi-autonomous underwater vehicle, *Ocean Eng*., **32**(13): 1631−1641.

Lin, C. F. and Wang, S. D., 2002. Fuzzy support vector machines, *IEEE Transactions on Neural Networks*, **13**(2): 464−471.

Lin, C. L., Feng, X. S. and Li, Y. P., 2011. Research on actuator fault detection of unmanned underwater vehicle based on unscented Kalman filter, *Machinery Design and Manufacture*, **5**, 168−170. (in Chinese)

Liu, X. M., Liu, G. J. and Qiu, J., 2006. Decision improving of unsupervised SVM for fault identification, *Chinese Journal of Mechanical Engineering*, **42**(4): 107−111. (in Chinese)

Peng, M. J. and Xiao, J. H., 2009. Dynamic SVDD algorithm and its application, *Computer Science*, **36**(3): 156−158. (in Chinese)

Qi, J. T. and Han, J. D., 2007. Fault diagnosis and fault-tolerant control of rotorcraft flying robots: A survey, *CAAI Transactions on Intelligent Systems*, **2**(2): 31−39.

Schwenker, F., 2000. Hierarchical support vector machines for multi-class pattern recognition, *Proc. 4th International Conference on Knowledge Based Intelligent Engineering System and Allied Technologies*, Brighton, 561−565.

Talebi, H. A., Khorasani, K. and Tafazoli, S., 2009. A recurrent neural-network based sensor and actuator fault detection and isolation for nonlinear systems with application to the satallite's attitude control subsystem, *IEEE Transactions on Neural Networks*, **20**(1): 45−60.

Tax, D. M. J. and Duin, R. P. W., 1999. Support vector domain description, *Pattern Recognition Letters,* **20**(11-13): 1191−1199.

Wang, S. W., Shi, X. H. and Xu, H., 2010. Fault diagnosis of UV's sensors based on wavelet neural network, *Journal of Test and Measurement Technology*, **24**(4): 367−371. (in Chinese)

Wei, X. K., Lu, B., Wang, C., Lu, J. M. and Li, Y. H., 2004. Applications of support vector machines to aeroengine fault diagnosis, *Journal of Aerospace Power*, **19**(6): 844−848. (in Chinese)

Weston, J. and Wathkins, C., 1998. *Multi-class Support Vector Machines*, Technical Report, Department of Computer Science, Royal Holloway, University of London.

Xu, Y. R. and Su, Y. M., 2008. Think on the development in autonomous underwater vehicles, *Ship Science and Technology*, **30**(1): 17−21. (in Chinese)

Xu, Y. R. and Xiao, K., 2007. Technology development of autonomous ocean vehicle, *Acta Autonomous Sinica*,

33(5): 518−521. (in Chinese)

Zhang, M. J., Wu, J. and Wang, Y. J., 2010. A method of multi-sensor simultaneous faults detection for autonomous underwater vehicle, *Robot*, **32**(5): 298−305. (in Chinese)

Zhang, Q., Xu, G. H., Wang, J. and Liang, L., 2007. Dynamic multi-fault diagnosis model based on support vector domain description, *Journal of Xi'an Jiaotong University*, **41**(5): 593−597. (in Chinese)

Zhang, Y., Liu. X. D., Xie, F. D. and Li, K. Q., 2009. Fault classifier of rotating machinery based on weighted support vector data description, *Expert Systems with Applications*, **36**(4): 7928−7932.

Zhou, S. L., Qin, L., Shi, X. J. and Xiao, Z. C., 2012. Hyper-sphere SVM and D-S theory for fault diagnosis, *Computer Engineering and Applications*, **48**(9): 6−9. (in Chinese)

Zhu, D. Q., Liu, Q. and Hu, Z., 2009. Reliability control technology of unmanned underwater vehicles, *Shipbuilding of China*, **50**(2): 183−192. (in Chinese)